Synthesis of Silicon Nanoparticles in a Novel CO_2 Laser Pyrolysis Reactor With an Elongated Reaction Zone

Seok-Ho Maeng
Kangwon National University
Hakju Lee
Kangwon National University
Seongbeom Kim (sbkim81@kangwon.ac.kr)
Kangwon National University - Samcheok Campus https://orcid.org/0000-0002-6495-2479

Nano Express

Keywords: Nanoparticle, Nanocrystal, Laser pyrolysis, Silicon, Synthesis reactor, Nanoparticle synthesis, CO2 laser synthesis

Posted Date: December 1st, 2020

DOI: https://doi.org/10.21203/rs.3.rs-114207/v1

Abstract

We demonstrated silicon nanoparticle synthesis using a novel CO_2 laser pyrolysis reactor. The reactor was designed to have an elongated reaction zone more than 10 times longer than conventional laser pyrolysis systems. Such elongation was achieved by aligning the laser beam and precursor gas stream. SiH_4 gas was used to synthesize the silicon nanoparticles. The yield of the nanoparticles was 40.9%, as calculated by comparing the masses of the synthesized nanoparticles and precursor gas used. Silicon nanoparticles synthesized by using a typical reactor with identical gas flow rate conditions and without a focusing lens had a nanoparticle yield of 1.7%, which was far smaller than for the new reactor. The average diameter of as-synthesized silicon nanoparticles was 26.7 nm. Considering that high power CO_2 lasers are often used for large scale nanoparticle production by laser pyrolysis, our proposed reactor serves as a proof of concept that demonstrates its potential for large scale nanoparticle synthesis.

Introduction

Laser pyrolysis techniques have been widely employed to synthesize nanoparticles ever since Haggerty *et al* reported the synthesis of silicon and silicon nitride nanoparticles.[1] This technique employs a CO_2 laser beam as a heat source and gaseous precursors as feedstock. The precursor molecules dissociate when the coupled energy provided by the laser beam is sufficient, which subsequently initiates the nucleation and growth of nanoparticles. These processes occur on timescales on the order of 10^{-3} seconds. The inherent characteristics of a laser beam make it an advantageous heat source for nanoparticle synthesis, specifically enabling contact-free, continuous, and high-yield processing of nanoparticles. In addition, process parameters such as the laser beam, precursor gases, and the pressure inside the reaction chamber can be independently controlled, thus enabling the judicious design and modification of processes to yield tailor-made nanoparticles. To date, the range of nanoparticles that can be produced by laser pyrolysis has steadily expanded. For instance, reports have exploited laser pyrolysis to generate silicon,[2–5] germanium,[6] silicon germanium alloy,[7,8] boron,[9] titanium oxide,[10] fullerene,[11] and iron oxide[12] nanoparticles. The versatility of the processing parameters permits various strategies for laser pyrolysis that can be employed to synthesize alloyed,[6,13] core-shell[14,15] and doped nanoparticles,[16,17] particularly by manipulating processing parameters or the configuration of the set-up.

Laser pyrolysis for the nanoparticle synthesis requires overlap of the cross-sectional areas of the incident laser beam and precursor gases. A typical set-up is configured to allow the laser to intersect the precursor gases orthogonally, with the cross-sectional area defining the reaction zone. The laser beam is focused by using an optical lens to increase the laser intensity in the reaction zone, unless the power of the unfocused laser beam is sufficient, *e.g.* greater than ~ 10^3 Watt. The reaction time and the reaction zone are limited to small values that hinder the use of various gases as precursors. Additional photosensitizer gases can be used, in particular when there is insufficient absorption cross-section between precursor gases and the laser beam. But including photosensitizer molecules potentially introduces contaminants. From a practical viewpoint, intensifying the laser beam promotes the nanoparticle synthesis by improving

nanoparticle yield, but causes thermal lensing effects[18] or thermal damage to the optical components[19] that are problematic and occur more frequently at increased laser intensities.

In this paper, we proposed a novel reactor that was designed with an elongated reaction zone that is more than 10 times longer than conventional laser pyrolysis systems. Such elongation was achieved by aligning the laser beam and precursor gas stream as shown in Fig. 1(a). By comparison, typical laser pyrolysis reactors have a much smaller reaction zone that is located at the intersection of the focused laser beam and precursor gas stream line, as shown in Fig. 1(b). The length of the reaction zone is approximately 180 mm in the new reactor which is much longer than that of typical reactor set-up with a few mm.

Results And Discussion

The CO_2 laser beam had a diameter of 4 ± 1 mm and operated at a wavelength of 10.6 μm, under continuous wave conditions, and without a focusing lens. A laser power of 57W was used, which was 95% of the maximum laser power. The nozzle system of the new reactor had three ports. Inert gas (N_2) is flowed through the bottom and the upper nozzles. The N_2 gas from the bottom nozzle prevents the deposition of nanoparticles and chemical reactions involving the precursor gas on the ZnSe window. The N_2 gas from the upper nozzle guides and confines the precursor gases. The N_2 gas flow rates were 150 and 5000 standard cubic centimeters per minute (sccm) at the bottom and upper nozzle, respectively. Precursor gas, which was SiH_4 here, was introduced into the reactor from the middle nozzle at a flow rate of 50 sccm. The flow rates of all gases were controlled by mass flow controllers. The body of the reactor could be designed in a cylindrical shape as shown in Fig. 1(a) because the gas mixtures and the laser beam were aligned in the same way. Therefore, the middle part of the reactor was built with a quartz tube in order to observe and monitor the reaction zone. A rotary vacuum pump was connected to the exhaust of the reactor. The gas mixture was eventually purified through a dry gas scrubber. The pressure inside the reactor was 400 Torr. Synthesized nanoparticles were captured in a membrane filter in the collector, which was installed between the reactor and a rotary vacuum pump. After synthesis, the collector was separated from the reactor system and transferred to an N_2-filled glove box to avoid exposure to the oxidizing effects of air.

As soon as the synthesis process initiated, it was able to observe red straight light through the quartz tube which was from the laser diode pointer (635 nm wavelength) scattered by the synthesized nanoparticles. However, strong reaction flame was not observed. Typically, bright reaction flame is observable at the confined reaction zone in the conventional reactor due to the thermal radiation from the heated solids or liquids.[4] Fig. 2 shows images of as-synthesized silicon nanoparticles prepared by using the new reactor. Images of silicon nanoparticles that were captured on the membrane filter are shown in Fig. 2(a). Silicon nanoparticles were densified and deposited on to the membrane. These nanoparticles were brown in color and were easily separated from the membrane as shown in Fig. 2(b). The yield of the nanoparticles was 40.9%, as calculated by comparing the masses of the synthesized nanoparticles and

precursor gas used. To compare the production yield, we synthesized silicon nanoparticles by using a conventional reactor which configured as in Fig. 1(b). Identical experimental conditions including gas flow rates and the laser beam were applied to the synthesis. The production yield of silicon nanoparticles was 1.7%, which was far smaller than for the new reactor. In conventional laser pyrolysis reactors, increases in either the laser beam intensity or density of precursor molecules lead to higher nanoparticle yields. Thus, collectively, these results demonstrate that the elongated reaction zone of the new reactor dramatically enhances the yield of silicon nanoparticles, especially at low laser intensities.

Transmission electron microscopy (TEM) images of the as-synthesized silicon nanoparticles are shown in Fig. 3. The silicon nanoparticles have quasi-spherical shapes and are aggregated (Fig. 3(a)). Lattice fringes were clearly visible in the magnified TEM image provided in Fig. 3(b). The internal region of the nanoparticle appears to be polycrystalline, which we believe originates from individual nanoparticles merging while traveling through the elongated reaction zone. Most of nanoparticles were polycrystalline. It is assumed that the temperature of the reaction zone is insufficient to recrystallize the nanoparticles. X-ray diffraction (XRD) patterns of as-synthesized silicon nanoparticles (Fig. 4(a)) exhibit peak patterns that correspond to crystalline silicon. Calculations by using the Scherrer equation reveals that the size of the crystallites was 19 nm. Nanoparticle size was also established by measuring the sizes of 89 individual nanoparticles from several TEM images, yielding an average size of 26.7 nm. Such a large discrepancy in the estimates of average size from XRD and TEM is reasonable because small domains within crystallites contribute to broad XRD peaks that would favor smaller size estimates. Figure 4(b) shows a histogram of the sizes of 89 silicon nanoparticles measured from TEM images. Large aggregates of nanoparticles of various shapes with characteristic lengths greater than 50 nm were frequently observed in TEM images. Such aggregated nanoparticles are composed of a collection of individual nanoparticles, as opposed to a single homogeneous particle, due to insufficiently high temperatures in the reaction zone. The elongated reaction zone increases production yield dramatically, however, is assumed to promote the growth of inhomogeneous nanoparticles.

Conclusions

We have demonstrated silicon nanoparticle synthesis using a new reactor and it was confirmed that our proposed reactor extends the reaction zone and thus reaction time, which improves production yield. Considering that high power CO_2 lasers are often used for large scale nanoparticle production by laser pyrolysis, our proposed reactor serves as a proof of concept that demonstrates its potential for large scale nanoparticle synthesis. The low laser powers required in the new reactor also provide advantages with respect to maintaining the fidelity of optical components, which may be able to tolerate even higher laser powers that would be beneficial for large scale nanoparticle production. Moreover, the elongated reaction zone could permit sufficient reaction times for precursors that have low absorption coefficients when using CO_2 laser beams. This research presents and demonstrates a novel laser pyrolysis reactor that we believe will meaningfully impact progress in the field of nanoparticle synthesis.

Abbreviations

TEM
Transmission electron microscopy
sccm
Standard cubic centimeters per minute
XRD
X-ray diffraction

Declarations

Competing interests

The authors declare that they have no competing interests.

Funding:

This research was supported by 2015 Research Grant from Kangwon National University and National Research Foundation of Korea (NRF-2017R1C1B2011606).

Authors' contributions

S.K. conceived the main idea and wrote the manuscript, S.M., H.L. and S.K. carried out the experiments

Corresponding author

Seongbeom Kim

References

1. Danforth SC, Flint JH, Cannon WR, Haggerty JS (1979) Laser synthesis of silicon nitride powders. AIP Conference Proceedings 50:659 (https://doi.org/10.1063/1.31734).
2. Huisken F, Ledoux G, Guillois O, Reynaud C (2002) Light-emitting silicon nanocrystals from laser pyrolysis. Adv Mater 14:1861-1865 (https://doi.org/10.1002/adma.200290021).
3. Li X, He Y, Swihart MT (2004) Surface functionalization of silicon nanoparticles produced by laser-driven pyrolysis of silane followed by HF–HNO_3 etching. Langmuir 20:4720-4727 (https://doi.org/10.1021/la036219j).
4. Kim S, Hwang C, Park SY, Ko S, Park H, Choi WC, Kim JB, Kim DS, Park S, Kim JY (2014) High-yield synthesis of single-crystal silicon nanoparticles as anode materials of lithium ion batteries via photosensitizer-assisted laser pyrolysis. J Mater Chem A 2:18070-18075 (https://doi.org/10.1039/C4TA03358B).

5. Sourice J, Quinsac A, Leconte Y, Sublemontier O, Porcher W, Haon C, Bordes A, Vito ED, Boulineau A, Larbi SJS, Herlin-Boime N, Reynaud C (2015) One-step synthesis of Si@C nanoparticles by laser pyrolysis: high-capacity anode material for lithium-ion batteries. ACS Appl Mater Interfaces 7:6637-6644 (https://doi.org/10.1021/am5089742).
6. Kim S, Park SY, Jeong J, Kim G, Rohani P, Kim DS, Swihart MT, Kim JY (2015) Production of pristine, sulfur-coated and silicon-alloyed germanium nanoparticles via laser pyrolysis. Nanotechnology 26:305703 (https://doi.org/10.1088/0957-4484/26/30/305703).
7. Erogbogbo F, Liu T, Ramadurai N, Tuccarione P, Lai L, Swihart MT, Prasad PN (2011) Creating ligand-free silicon germanium alloy nanocrystal inks. ACS Nano 5:7950-7959 (https://doi.org/10.1021/nn2023304).
8. Ge M, Kim S, Nie A, Shahbazian-Yassar R, Mecklenburg M, Lu Y, Fang X, Shen C, Rong J, Park SY, Kim DS, Kim JY, Zhou C (2015) Capacity retention behavior and morphology evolution of Si_xGe_{1-x} nanoparticles as lithium-ion battery anode. Nanotechnology 26:255702 (https://doi.org/10.1088/0957-4484/26/25/255702).
9. Rohani P, Kim S, Swihart MT (2016) Boron nanoparticles for room-temperature hydrogen generation from water. Adv Energy Mater. 6:1502550 (https://doi.org/10.1002/aenm.201502550).
10. Belchi R, Habert A, Foy E, Gheno A, Vedraine S, Antony R, Ratier B, Bouclé J, Herlin-Boime N (2019) One-step synthesis of TiO_2/graphene nanocomposites by laser pyrolysis with well-controlled properties and application in perovskite solar cells. ACS Omega 4:11906-11913 (https://doi.org/10.1021/acsomega.9b01352).
11. Mordkovich VZ (2000) The observation of large concentric shell fullerenes and fullerene-like nanoparticles in laser pyrolysis carbon blacks. Chem Mater 12:2813-2818 (https://doi.org/10.1021/cm0001814).
12. Morales MP, Bomati-Miguel O, Perez De Alejo R, Ruiz-Cabello J, Veintemillas-Verdaguer S, O'Grady K (2003) Contrast agents for MRI based on iron oxide nanoparticles prepared by laser pyrolysis. J Magn Magn Mater 266:102-109 (https://doi.org/10.1016/S0304-8853(03)00461-X).
13. Martinez G, Malumbres A, Lopez A, Mallada R, Hueso JL, Santamaria J (2018) Laser-assisted production of carbon-encapsulated Pt-Co alloy nanoparticles for preferential oxidation of carbon monoxide. Front Chem 6:487 (https://doi.org/10.3389/fchem.2018.00487).
14. Dumitrache F, Morjan I, Alexandrescu R, Ciupina V, Prodan G, Voicu I, Fleaca C, Albu L, Savoiu M, Sandu I, Popovici E, Soare I (2005) Iron–iron oxide core–shell nanoparticles synthesized by laser pyrolysis followed by superficial oxidation. Appl Surf Sci 247:25-31 (https://doi.org/10.1016/j.apsusc.2005.01.037).
15. Fleacă C, Dumitrache F, Dutu E, Luculescu C, Niculescu A, Ilie A, Vasile E (2016) One step synthesis of tin-carbon core-shell nanoparticles using laser pyrolysis technique. U P B Sci Bull Series B 78:43-56.
16. Wang LP, Leconte Y, Feng Z, Wei C, Zhao Y, Ma Q, Xu W, Bourrioux S, Azais P, Srinivasan M (2017) Novel preparation of N-doped SnO_2 nanoparticles via laser-assisted pyrolysis: demonstration of

exceptional lithium storage properties. Adv Mater 29:1603286 (https://doi.org/10.1002/adma.201603286).

17. Rohani P, Banerjee S, Sharifi-Asl S, Malekzadeh M, Shahbazian-Yassar R, Billinge SJL, Swihart MT (2019) Synthesis and properties of plasmonic boron-hyperdoped silicon nanoparticles. Adv Funct Mater 29:1807788 (https://doi.org/10.1002/adfm.201807788).
18. Miyamoto I, Nanba H, Maruo H (1990) Analysis of thermally induced optical distortion in lens during focusing high-power CO_2 laser beam. Proc SPIE, CO_2 Lasers and Applications II 1276:112 (https://doi.org/10.1117/12.20537).
19. Puttick KE, Holm R, Ristau D, Natzschka U, Kiriakidis G, Garawal N, Judd E, Holland D, Greening D, Ellis N, Wilkinson M, Pamies MG, Sanviti C (1998) Continuous-wave CO_2-laser-induced damage thresholds in optical components. Proc SPIE, Laser-Induced Damage in Optical Materials 3244:188 (https://doi.org/10.1117/12.307045).

Figures

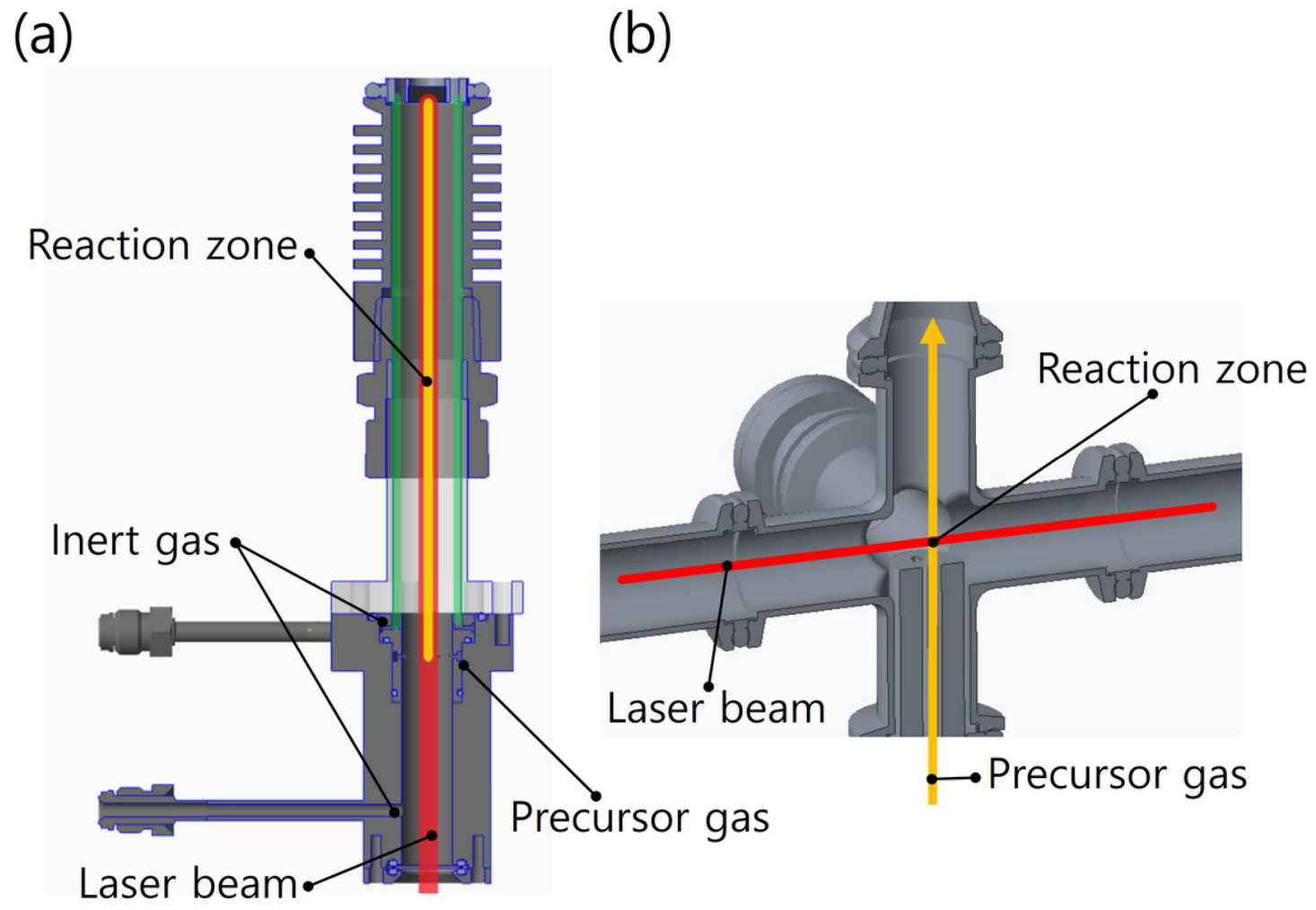

Figure 1

Schematics of (a) the novel laser pyrolysis reactor with an elongated reaction zone and (b) a conventional laser pyrolysis reactor.

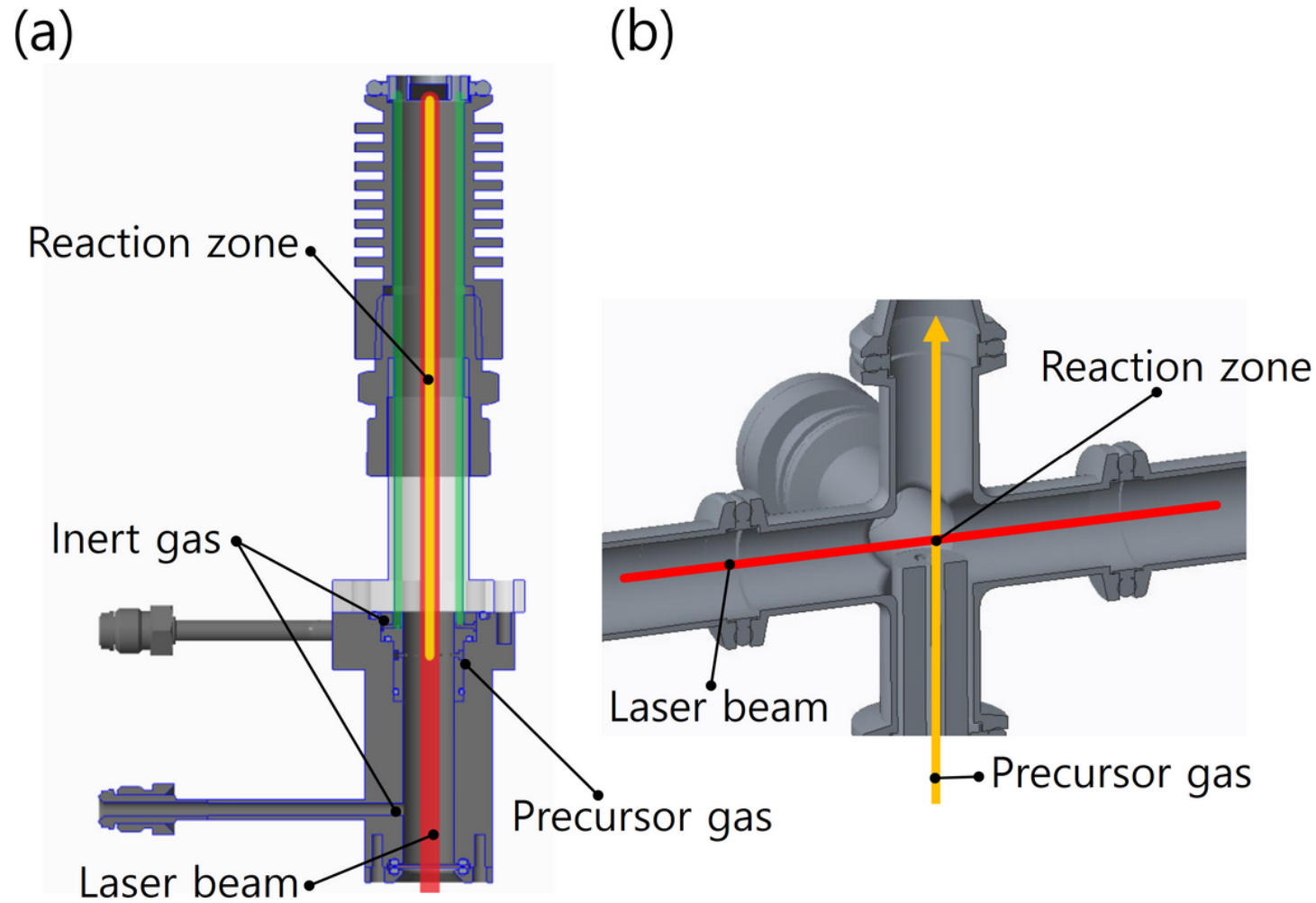

Figure 1

Schematics of (a) the novel laser pyrolysis reactor with an elongated reaction zone and (b) a conventional laser pyrolysis reactor.

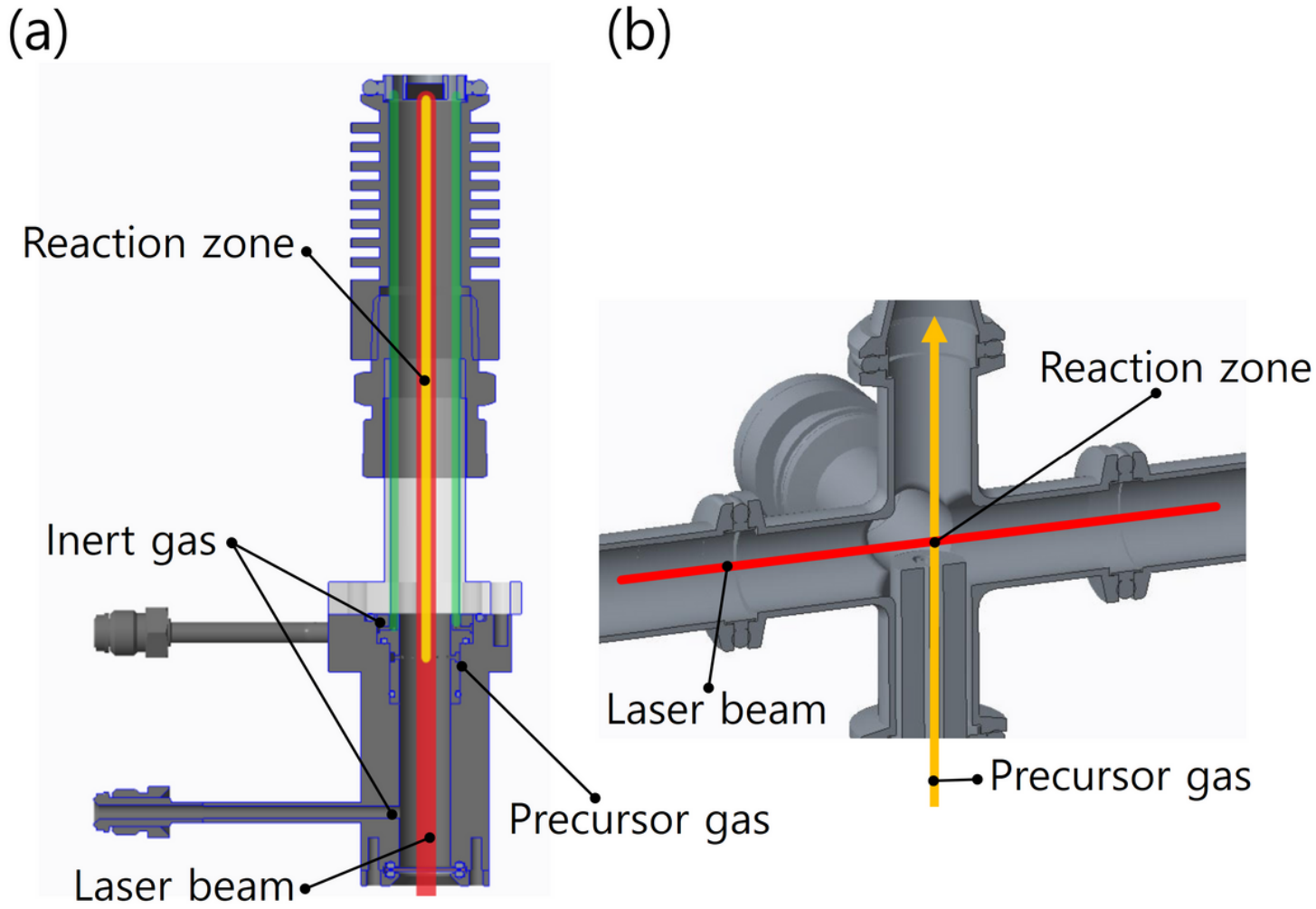

Figure 1

Schematics of (a) the novel laser pyrolysis reactor with an elongated reaction zone and (b) a conventional laser pyrolysis reactor.

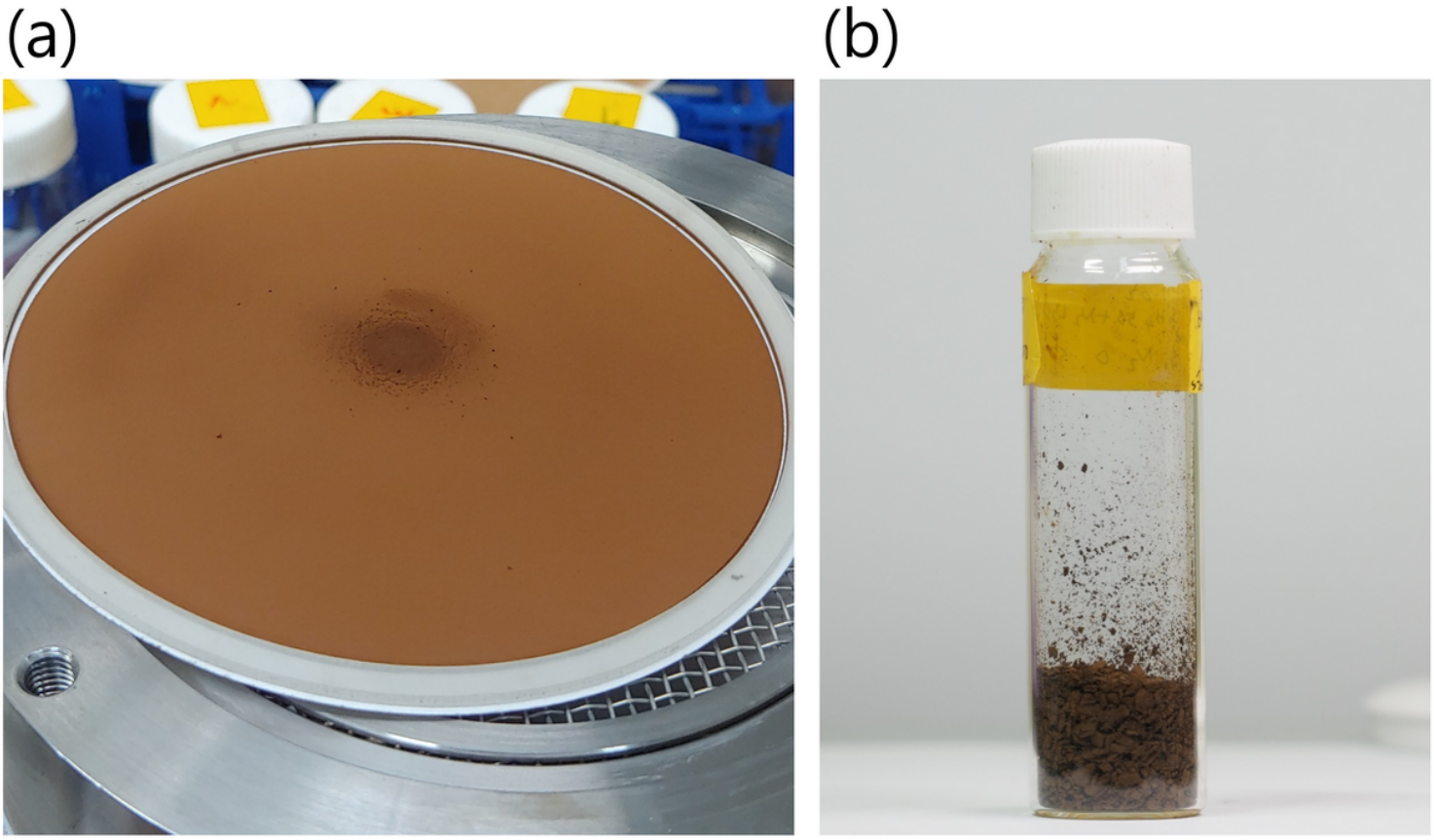

Figure 2

Optical images of as-synthesized silicon nanoparticles on (a) the membrane filter and (b) collected in a glass vial.

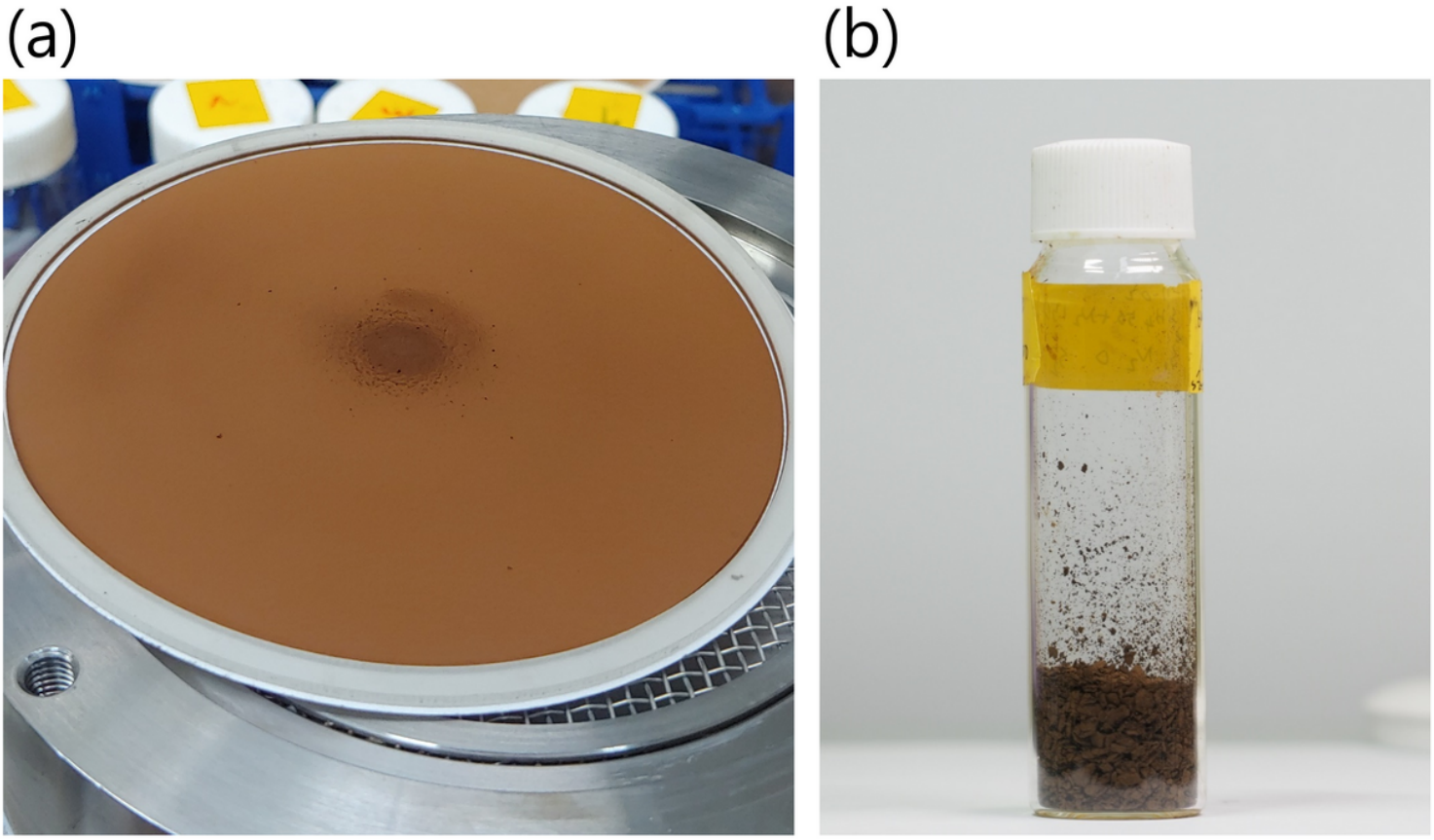

Figure 2

Optical images of as-synthesized silicon nanoparticles on (a) the membrane filter and (b) collected in a glass vial.

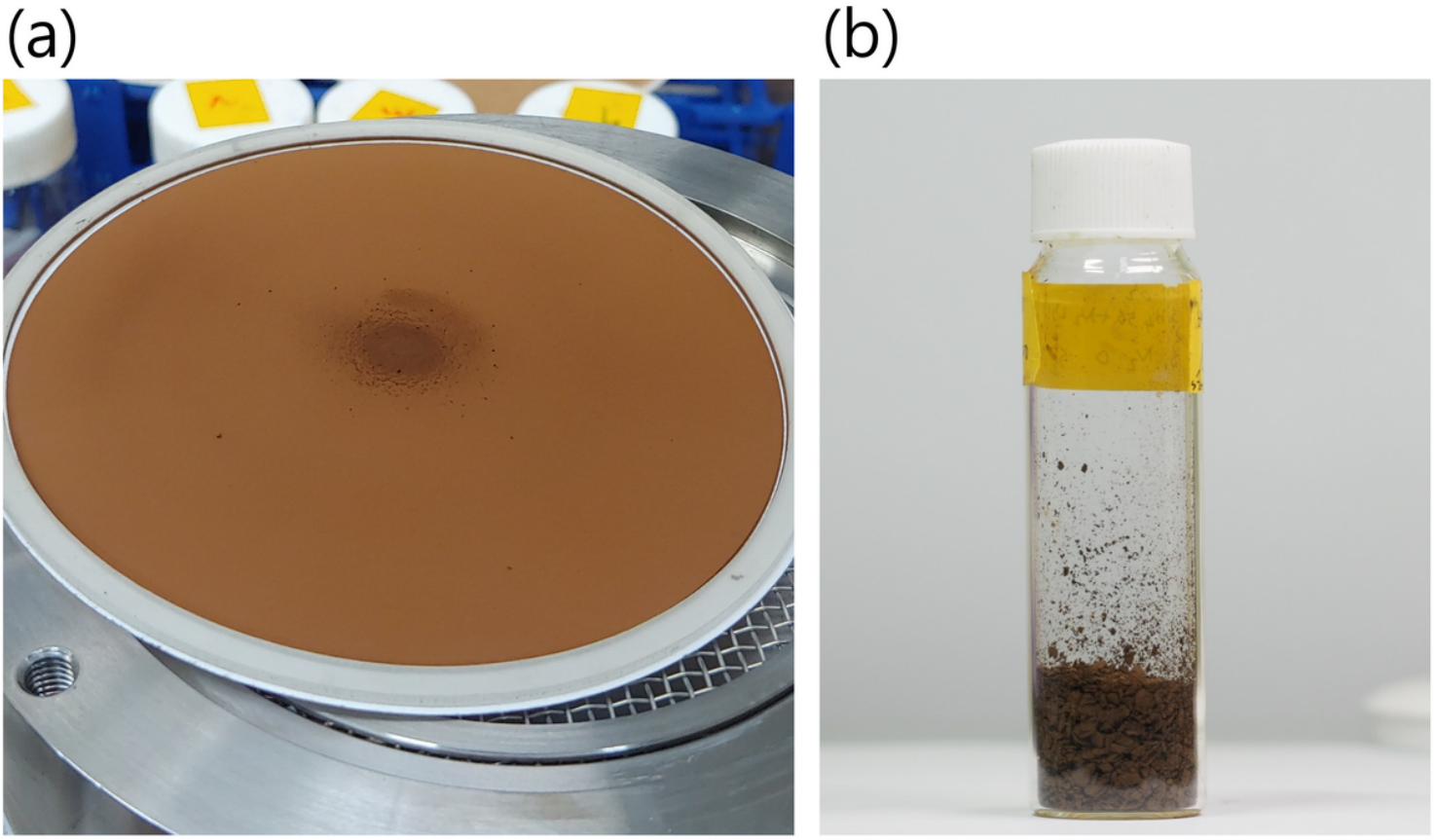

Figure 2

Optical images of as-synthesized silicon nanoparticles on (a) the membrane filter and (b) collected in a glass vial.

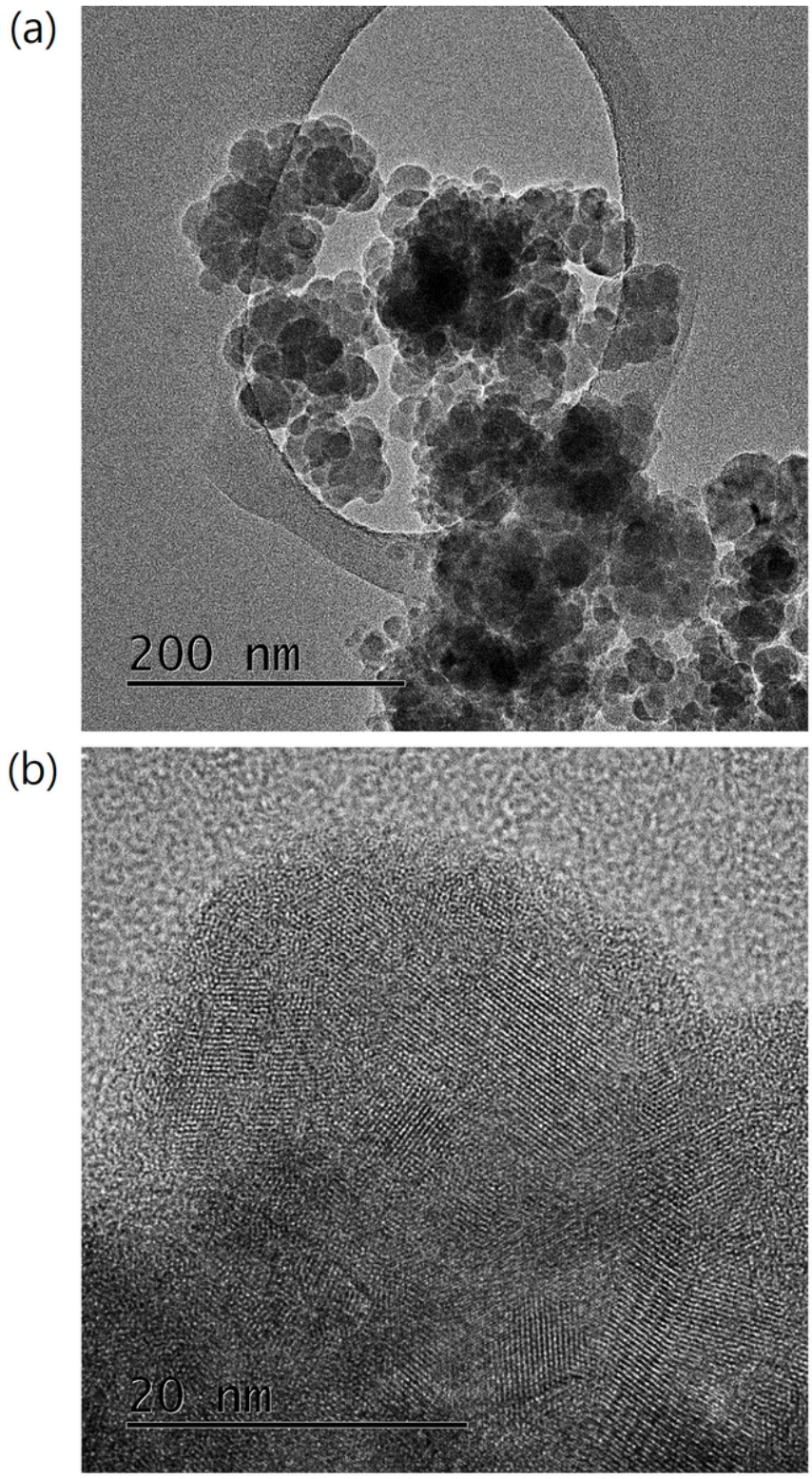

Figure 3

TEM images of the as-synthesized silicon nanoparticles with (a) low magnification and (b) high magnification.

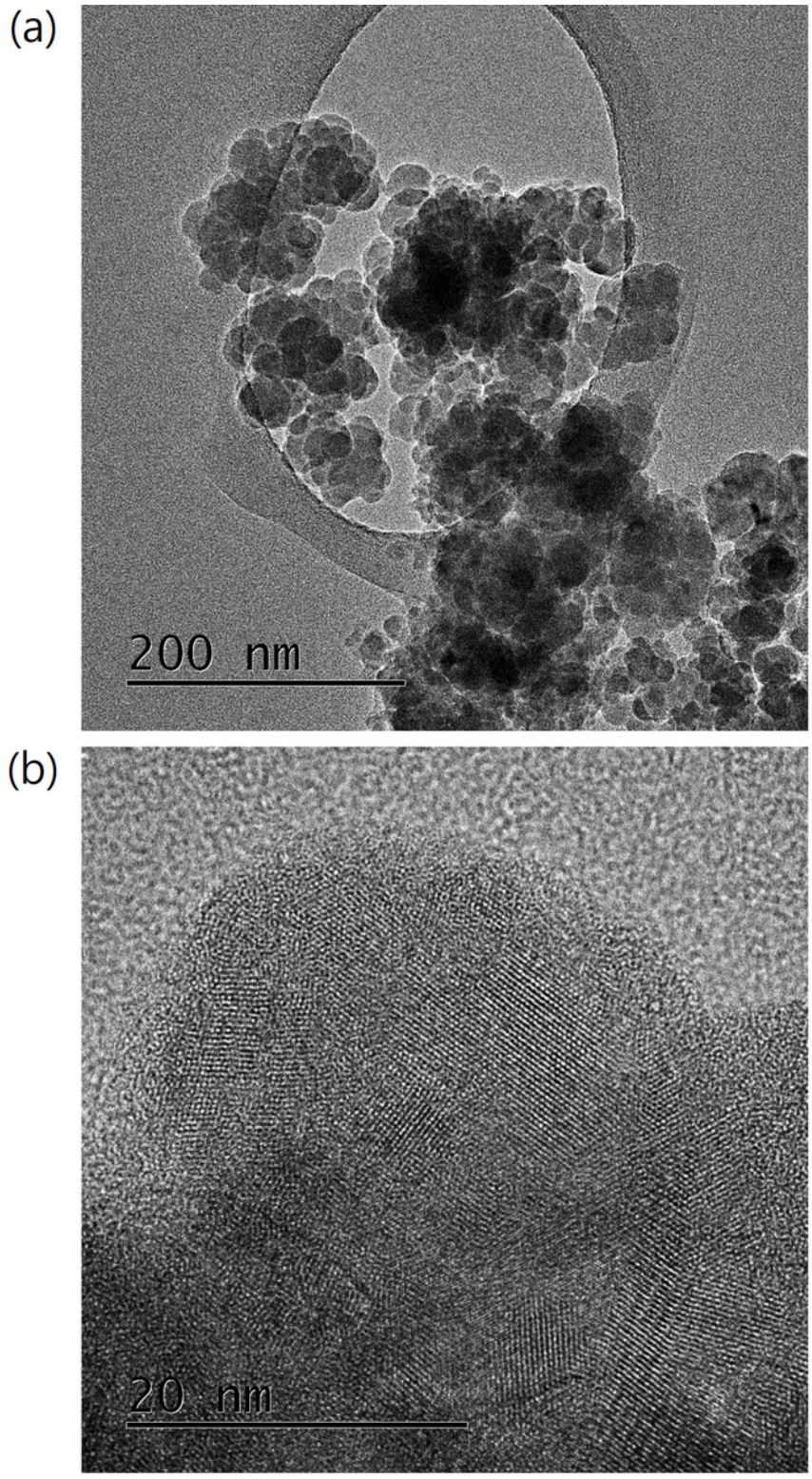

Figure 3

TEM images of the as-synthesized silicon nanoparticles with (a) low magnification and (b) high magnification.

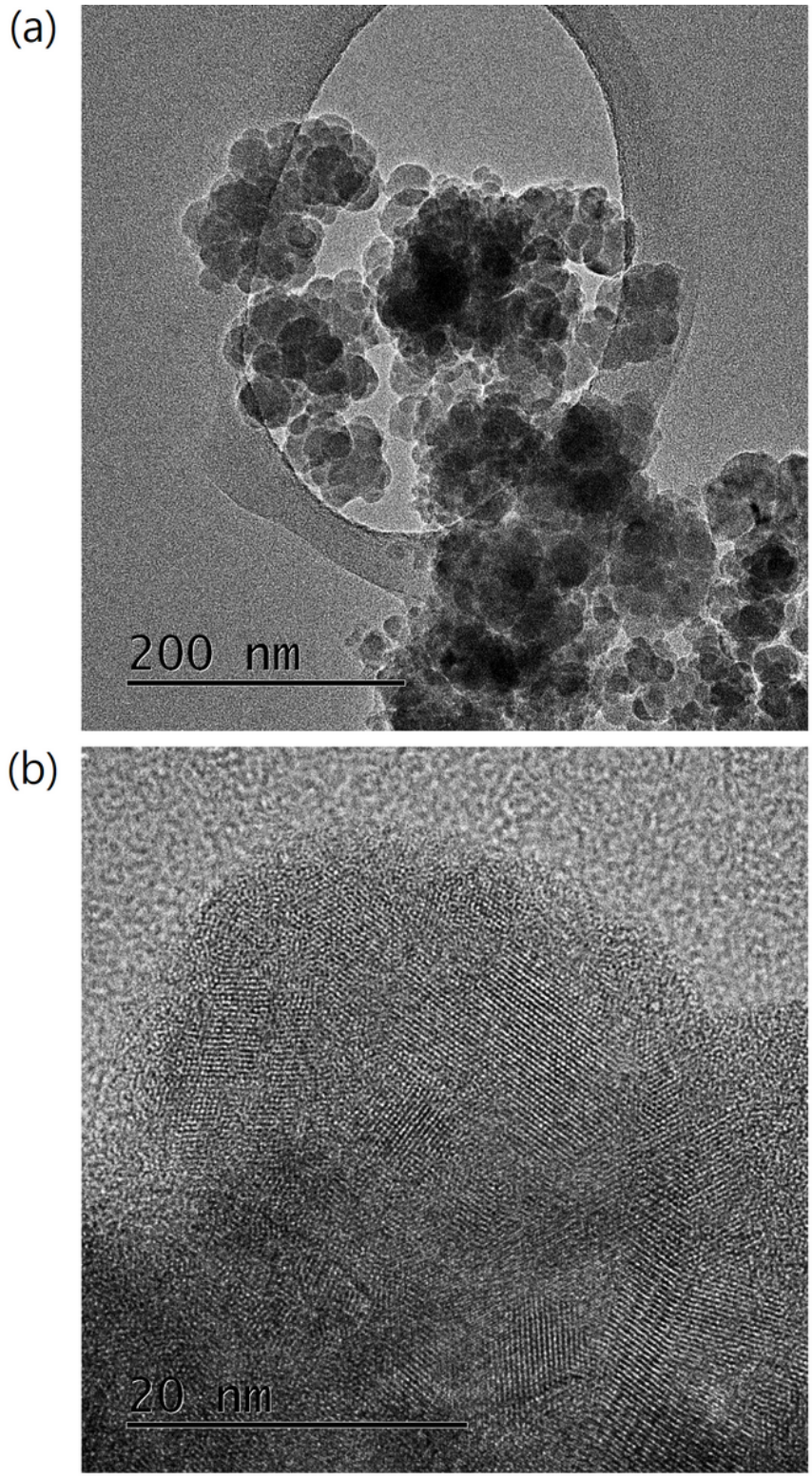

Figure 3

TEM images of the as-synthesized silicon nanoparticles with (a) low magnification and (b) high magnification.

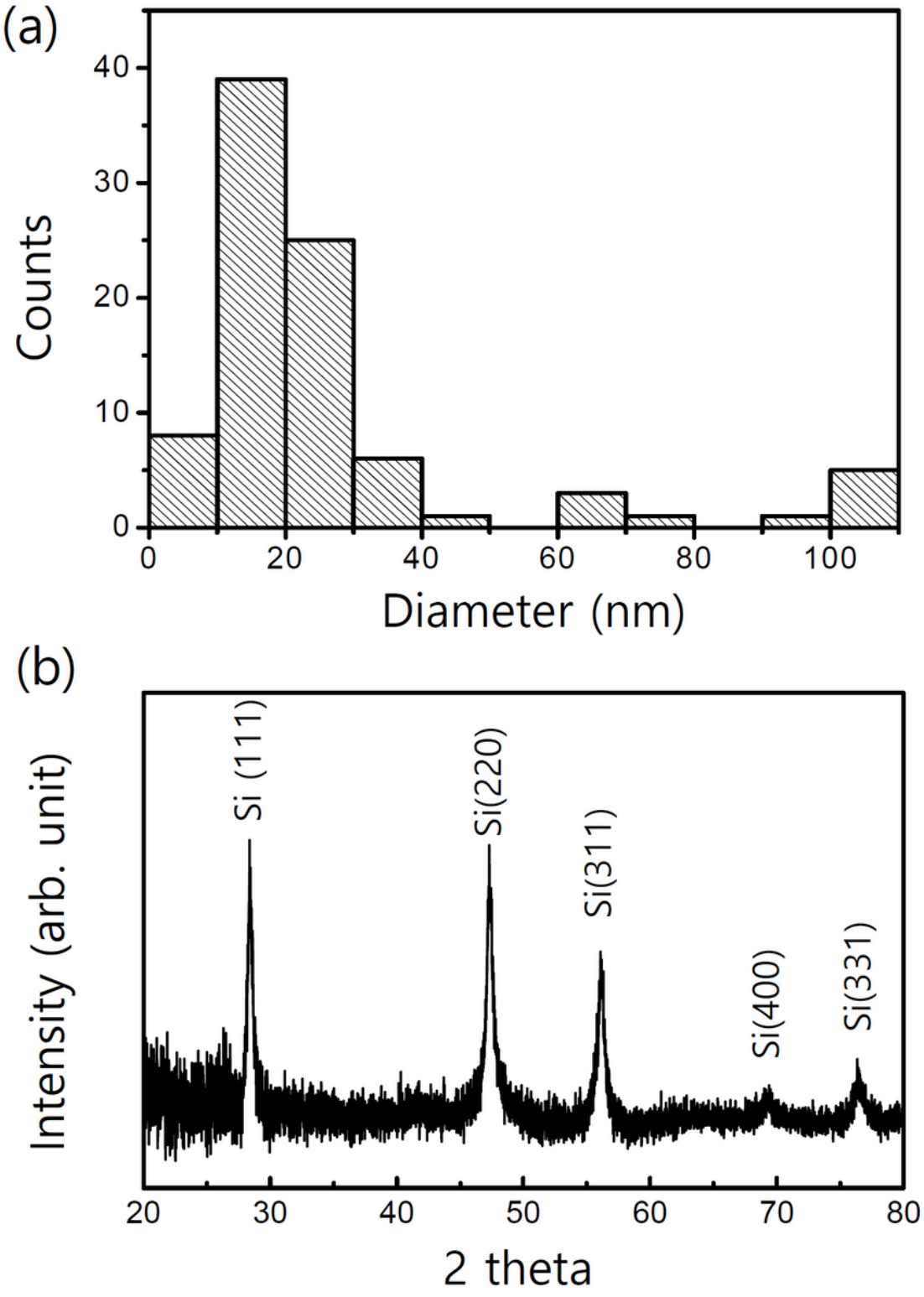

Figure 4

(a) A histogram of the nanoparticle size distribution and (b) XRD patterns of as-synthesized silicon nanoparticles.

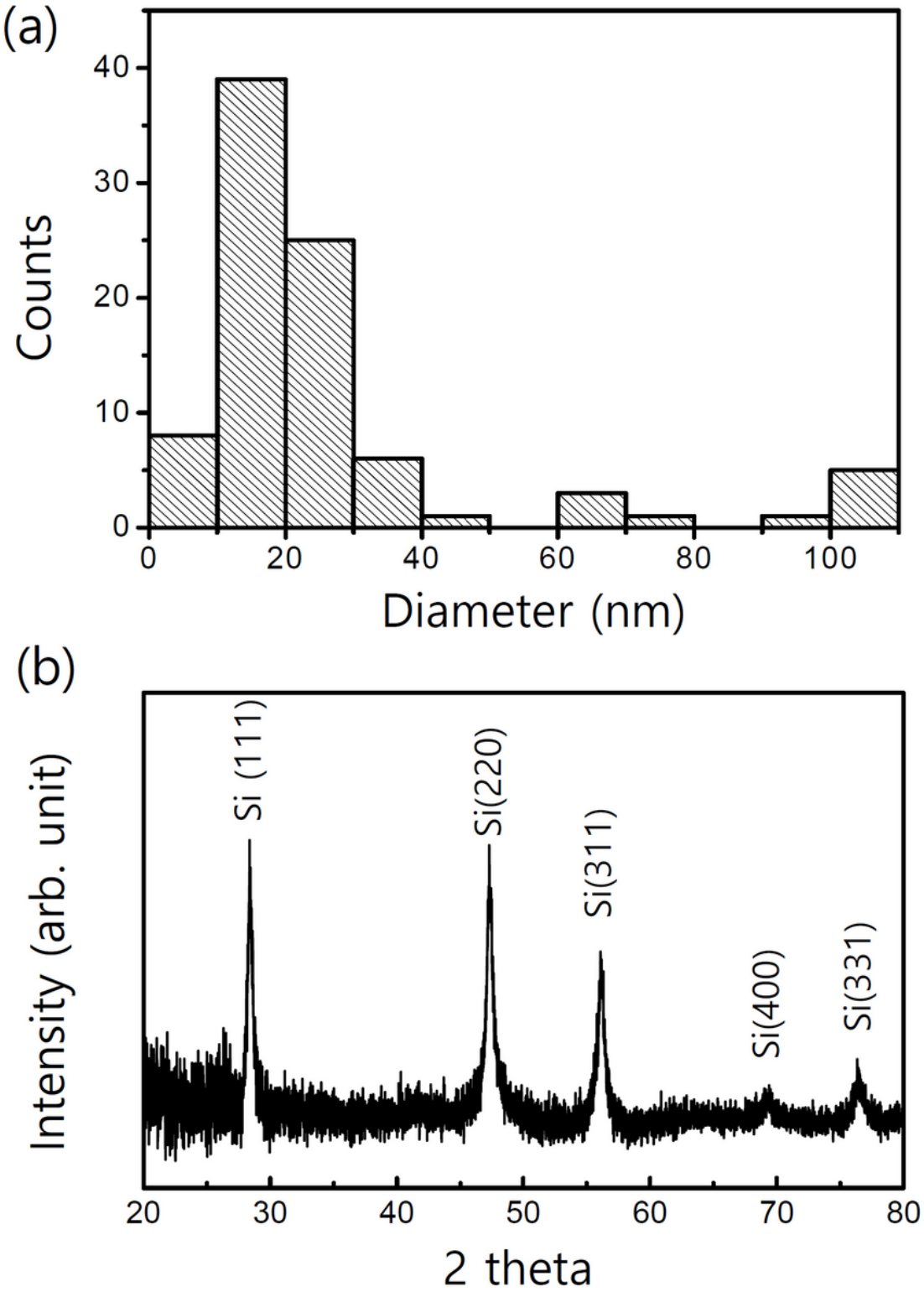

Figure 4

(a) A histogram of the nanoparticle size distribution and (b) XRD patterns of as-synthesized silicon nanoparticles.

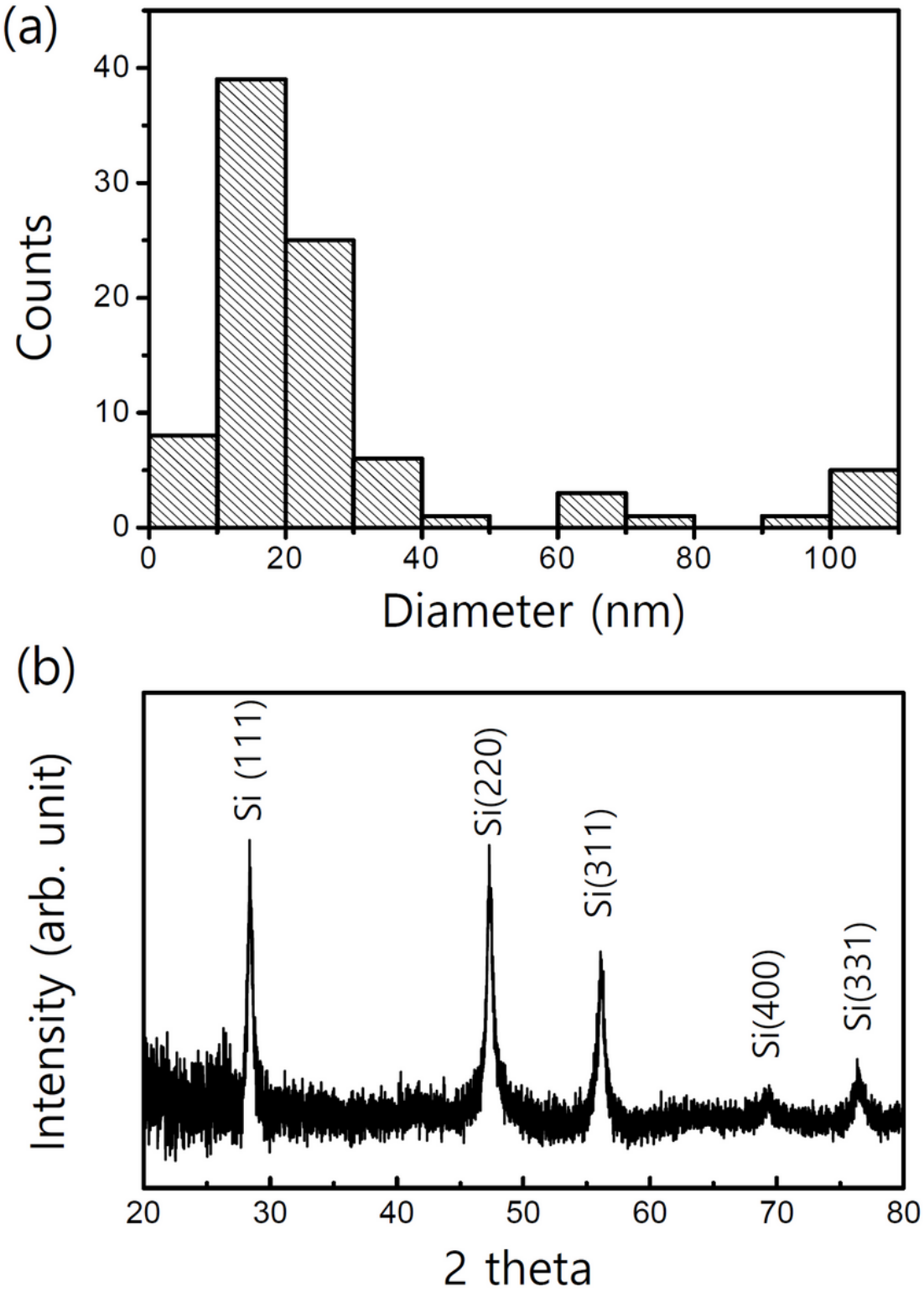

Figure 4

(a) A histogram of the nanoparticle size distribution and (b) XRD patterns of as-synthesized silicon nanoparticles.